Frequency-fluctuation model applied to Stark-Zeeman spectral line shapes in plasmas

S. Ferri,* A. Calisti, C. Mossé, L. Mouret, and B. Talin
Laboratoire PIIM, UMR 6633, Université de Provence-CNRS, Centre de Saint Jérôme, Case 232, F-13397 Marseille Cedex 20, France

M. A. Gigosos and M. A. González
Departamento de Óptica y Física Aplicada, Facultad de Ciencias, Universidad de Valladolid, E-47071 Valladolid, Spain

V. Lisitsa
Russian Research Center, Kurchatov Institute, Moscow RU-123182, Russia

(Received 15 January 2010; revised manuscript received 4 February 2011; published 18 August 2011)

A very fast method for calculating line shapes in the presence of an external magnetic field accounting for charge particle dynamics is proposed. It is based on a reformulation of the frequency fluctuation model, which provides an expression of the dynamic line shape as a functional of the static distribution function of frequencies. In the presence of an external magnetic field, the distribution of intensity and polarization of the emission depends on the angle between the observation line and the magnetic field's direction. Comparisons with numerical simulations and experimental results for various plasma conditions show very good agreement. Results on hydrogen lines in the context of magnetic fusion and the Lyman-α line, accounting for fine structure, emitted by argon in the context of inertial fusion, are also presented.

DOI: 10.1103/PhysRevE.84.026407 PACS number(s): 52.20.−j, 32.70.Jz, 32.60.+i, 52.25.−b

I. INTRODUCTION

The presence of a static magnetic field is common for many types of plasmas and revives the interest for modeling the line shapes affected simultaneously by Stark and Zeeman effects. Such a combined influence on profiles of spectral lines has been studied for several decades both theoretically and experimentally since the initial work [1]. Different methods have been developed or have been extended to magnetic plasmas, such as numerical simulations [2–4] and theoretical models [5–12]. The aim of the latter is to give a rapid and accurate description of the line shapes or to be implemented in transport codes dedicated to plasma spectroscopy.

Modeling the broadening due to both the Stark and the Zeeman effects is a complex problem that requires the knowledge of accurate atomic physics data, statistical mechanics, and plasma physics. A magnetic field has three essential effects on Stark-broadened spectral lines: (1) partial polarization of the emitted light, (2) additional splitting caused by the magnetic field according to value of the magnetic quantum number m, and (3) bending of the electron trajectories into a helical path around the magnetic lines of forces. The third point will not be considered in this paper. The magnetic field leads to an additional structure in the line profile due to the energy level splitting. A measure of the relative importance of the Stark and Zeeman effects is given by the ratio τ between the two respective average energy shifts [1]. For hydrogen, with the normal field strength $F_0 = 2.603eN_e^{2/3}$, τ is as follows:

$$\tau = 5.15 \times 10^{-11} n N_e^{2/3}/B, \qquad (1)$$

where n is the principal quantum number, N_e is the electron density, expressed in cm^{-3}, and B is the magnetic field strength, expressed in teslas. The line profile coincides with the pure Stark profile if $\tau \gg 1$ and deviates progressively as τ decreases. When $\tau \approx 1$, profiles broadened by the combined Stark-Zeeman effect are an intricate function of N_e and B. Such cases are found in magnetically confined plasmas for low-n hydrogen lines emitted in the divertor region at $N_e > 10^{14}\ \mathrm{cm}^{-3}$, $kT_e \sim 1$ eV, and $B \simeq$ few teslas. In plasmas produced by laser impact or implosion (temperatures from 100 to 1000 eV and electron densities from 10^{21} to $10^{24}\ \mathrm{cm}^{-3}$), high magnetic fields ($B > 100$ T) are generated that can strongly affect the emission of highly ionized atoms. These conditions are favorable for the combined Stark-Zeeman effect on line profiles, not to mention astrophysical plasmas where the signature of uniform magnetic fields is observed on hydrogen lines in regions where $N_e \sim 10^{14}\ \mathrm{cm}^{-3}$ and $kT_e \sim 1$ eV (see Ref. [6] and references therein).

The most difficult part of the line broadening problem is to properly identify the environment of the emitter. In particular, accounting for the fluctuations of electric fields produced at emitters, by moving electrons and ions, is a nontrivial problem that has been of constant interest for both experimental and theoretical points of view since the 1960s (see Ref. [7] and references therein). Moreover, the presence of a static magnetic field, by giving a preferential axis, imposes the orientation of the electric dipole and can alter the dynamical properties of the plasma. Few models accounting for both the magnetic and the fluctuating electric fields have been developed [6,8,12,13]. Here, a method based on a reformulation of the frequency fluctuation model (FFM) [14], extended to magnetized plasmas, is presented.

II. METHOD

The line shape function in the radiative dipole approximation is related to the imaginary part of the Fourier-transformed dipole autocorrelation function. This can be written as a

*sandrine.ferri@univ-provence.fr

normalized Liouville space-matrix element of the response function,

$$I(\omega) = \mathrm{Im}\langle\langle \mathbf{d}^\dagger | G(\omega) | \mathbf{d}\rho_0 \rangle\rangle, \tag{2}$$

with ρ_0 as the equilibrium density matrix operator and $\mathbf{d}$ as the dipole operator for the emitting system. The response function $G(\omega - i\varepsilon)$ is given by the one-sided Fourier transform of the bath averaged evolution operator of the emitter $U(t)$,

$$G(\omega) = \lim_{\varepsilon \to 0} i \int_0^{+\infty} U(t) e^{-i(\omega - i\varepsilon)t} dt. \tag{3}$$

$U(t) = \langle U_l(t) \rangle_{l \in \{F\}}$ with $U_l(t)$ as the solution of the following equation:

$$\frac{dU_l(t)}{dt} = -i L_l(t) U_l(t) \quad \text{and} \quad U_l(0) = \mathbf{1}. \tag{4}$$

Here, $\mathbf{1}$ is the unit operator and $L_l(t)$ is the sum of three terms: $L_l(t) = L_0 + l(t) + L_Z$, where L_0 describes the behavior of the unperturbed atom and where $l(t)$ and L_Z are the Liouvillians corresponding to the Stark and Zeeman effects, respectively. The latter are treated as perturbations to L_0. Here:

(i) $l(t) = -\frac{1}{\hbar}\mathbf{d} \cdot \mathbf{F}_l(t)$ is the time dependent Liouville perturbation operator that connects the quantum emitter via the dipole operator $\mathbf{d}$ to the external electric field $\mathbf{F}_l(t)$. The latter is assumed to belong to a measurable functional space $\{F\}$ that provides a statistical method for the calculation of average quantities,

(ii) and L_Z is written as $L_Z = \frac{1}{\hbar}\mu_B \mathbf{B} \cdot [\mathbf{J} + (g_S - 1)\mathbf{S}]$, with the spin $\mathbf{S}$ and the angular momentum $\mathbf{J}$; $g_S \cong 2.002\,32$ is the anomalous gyromagnetic ratio for the electron spin. Here, the diamagnetic term, proportional to B^2, is assumed negligible compared to the paramagnetic term, proportional to B, and is not taken into account.

Due to the stochastic behavior of the electric field, $U(t)$ can be obtained by numerical simulation integrating Eq. (4) on a simulated sampling of $\{F\}$. Alternatively, efficient analytical models (e.g., the quasistatic approximation, the impact approximation, the model microfield method, the FFM, and the Boerker-Iglesias-Dufty model [7]) have been developed.

One feature of the Stark-Zeeman line shape modeling is a quantization axis imposed by the magnetic field. Averaging over $\mathbf{F}_l$ implies considering the three directions of space separately. Considering the magnetic field in the direction z, i.e., $\mathbf{B} = B\mathbf{e_z}$, one can define $\mathbf{F}_\parallel$ and $\mathbf{F}_\perp$ as the microfield parallel and perpendicular, respectively, to the direction of the magnetic field.

The selection rules for electric dipole radiation are as follows:

$$\Delta J = 0, \pm 1 (0 \nrightarrow 0), \quad \Delta M = \begin{cases} \pm 1, & \sigma \text{ components}, \\ 0, & \pi \text{ component}, \end{cases} \tag{5}$$

with M as the magnetic quantum number. By observing perpendicular to the magnetic field, the σ and π components show a linear polarization, respectively, parallel and perpendicular to $\mathbf{B}$. Along the $\mathbf{B}$ direction, the σ components show a circular polarization, and the π components do not appear. The profile observed in a direction with an angle α to the magnetic field is given by

$$I(\omega, \alpha) = I_\parallel \cos^2 \alpha + I_\perp \sin^2 \alpha, \tag{6}$$

where the parallel $I_\parallel$ and the transverse $I_\perp$ profiles are expressed in terms of polarized emission as

$$I_\parallel = I_+(\omega) + I_-(\omega), \tag{7}$$

$$I_\perp = \tfrac{1}{2}[I_+(\omega) + I_-(\omega)] + I_0(\omega). \tag{8}$$

Decomposing the dipole operator along the polarization vector basis $\{\mathbf{e}_q; q = 0, \pm 1\}$, the line intensity $I_q(\omega)$ associated with each polarization state is given by

$$I_q(\omega) = \mathrm{Im}\langle\langle \mathbf{d}_\mathbf{q}^\dagger | G(\omega) | \mathbf{d}_\mathbf{q} \rho_0 \rangle\rangle. \tag{9}$$

In the FFM, the line shape calculation is initially performed by treating the electron collisions as impacts and the ion perturbation as quasistatic [15]. The time dependence is introduced at a later stage of the calculation. Considering a static ionic electric field and electrons as impact results in a quantum-emitter system evolution operator $l = -\frac{1}{\hbar}\mathbf{d} \cdot \mathbf{F}_l + i\Phi_e$ containing a non-Hermitian homogeneous electron-impact broadening contribution Φ_e and the ion microfield interaction $-\frac{1}{\hbar}\mathbf{d} \cdot \mathbf{F}_l$, which has to be numerically averaged with a static-field probability distribution $Q(\mathbf{F}_l)$ [16]. The evaluation of the Liouville operator matrix elements requires the calculation of the electric dipole matrix elements $\langle \gamma J M | \mathbf{d_q} | \gamma' \mathbf{J}' \mathbf{M}' \rangle$ and the matrix elements $\langle \gamma J M | \mathbf{J_0} + \mathbf{S_0} | \gamma' \mathbf{J}' \mathbf{M}' \rangle$ related to the paramagnetic matrix elements of L_z with $\mathbf{B} = B\mathbf{e_z}$ and $g_S = 2$. The calculation can be simplified by using the Wigner-Eckart theorem [17]:

(i) the electric dipole matrix elements become

$$\langle \gamma J M | \mathbf{d_q} | \gamma' \mathbf{J}' \mathbf{M}' \rangle = (-1)^{J-M} \begin{pmatrix} J & 1 & J' \\ -M & q & M' \end{pmatrix} \times \langle \gamma J || \mathbf{d} || \gamma' \mathbf{J}' \rangle, \tag{10}$$

where $\langle \gamma J || \mathbf{d} || \gamma' \mathbf{J}' \rangle$ is the reduced matrix element,

(ii) and in the LS representation, the paramagnetic matrix elements become

$$\begin{aligned} &\langle \gamma J M | \mathbf{J_0} + \mathbf{S_0} | \gamma' \mathbf{J}' \mathbf{M}' \rangle \\ &= M \delta_{\gamma J M, \gamma' J' M'} - \delta_{\gamma L S M \gamma' L' S' M'} (-1)^{L+S+M} \\ &\quad \times [J, J']^{1/2} \sqrt{S(S+1)(2S+1)} \\ &\quad \times \begin{pmatrix} J & 1 & J' \\ -M & 0 & M \end{pmatrix} \begin{Bmatrix} L & S & J \\ 1 & J' & S \end{Bmatrix}. \end{aligned} \tag{11}$$

Here, the diagonal and off-diagonal ($J' = J - 1$) matrix elements are given by the analytical evaluation of the $3 - j$ and $6 - j$ symbols.

This implies the knowledge of J and S values of each state and the reduced matrix elements between states. Such information can be extracted from atomic structure codes (based on either LS or JJ coupling) [17–20].

In the absence of a magnetic field, models that rely on quasistatic approximation assume the plasma, surrounding the emitting atom, isotrope. The ion microfield distribution function is then a function of the ionic field strength, i.e., $W(F) = 4\pi F^2 Q(\mathbf{F})$. With the introduction of an external magnetic field, the symmetry is broken, and the integration over the electric field has to take it into account. If θ is the angle between the magnetic and the electric fields, then the parallel

and perpendicular components are defined by $F_\parallel = F_l\mu$ and $F_\perp = F_l\sqrt{1-\mu^2}$, where $\mu = \cos\theta$ and Eq. (9) is written as

$$I_q(\omega) = \int_0^\infty W(F_l)\int_{-1}^{1} J_q(F_l,\mu,\omega)\,d\mu\,dF_l, \qquad (12)$$

$J_q(F_l,\mu,\omega) = \mathrm{Im}\langle\langle \mathbf{d}_\mathbf{q}^\dagger \,|\, (\omega\mathbf{1} - L_0 - l - L_Z)^{-1} \,|\, \mathbf{d}_\mathbf{q}\rho_0\rangle\rangle$ represents the q-polarized intensity emitted by an ion in an external magnetic field and in a static ion field F_l having a direction μ compared to the magnetic field direction. In order to numerically treat Eq. (12), the integrations over F_l and μ are replaced by two weighted sums: Two-point integration weights $W_f^{(2)}$ are used for the summation over discrete ionic field intensities f, and Gauss-Legendre quadrature weights $W_\mu^{(G)}$, with the respective abscissa μ, are used for the angle summation [21,22]. Note that this discretization is possible because of the homogeneous electron broadening. Thus, the Fourier transform in Eq. (3) can be calculated in the $\{f,\mu\}$-dependent basis that makes the Liouville operator diagonal,

$$I_q(\omega)W = W\sum_f W_f^{(2)}\sum_\mu W_\mu^{(G)}\mathrm{Im}\big\langle\big\langle \mathbf{d}_\mathbf{q}^\dagger | M_{f,\mu} \times[\omega\mathbf{1} - L^d(f,\mu)]^{-1}M_{f,\mu}^{-1}|\mathbf{d}_\mathbf{q}\rho_0\big\rangle\big\rangle. \qquad (13)$$

Here, $M_{f,\mu}$ is the matrix that diagonalizes the Liouville operator L, $M_{f,\mu}^{-1}L(f,\mu)M_{f,\mu} = L^d(f,\mu)$. This procedure leads to the concept of the Stark spectral components emitted by a set of dressed two-level radiators [Stark-dressed transitions (SDTs)], which are defined by two complex numbers, the generalized intensity $a_{q,k} + ic_{q,k}$ and the generalized frequency $f_{q,k} + i\gamma_{q,k}$ (for more details, see Ref. [23]). Now, working in the Liouville space of the dressed two-level radiators, the static line shape is written [24]

$$I_q(\omega) = \mathrm{Re}\frac{1}{\pi}\sum_{kj} i\langle D_{q,k}|(\omega\mathbf{1} - L^d)^{-1}|D_{q,j}\rangle p_{q,j}, \qquad (14)$$

where L^d is the Liouville operator involving the transition frequencies of the SDT, $D_{q,j} = r_q\sqrt{1+ic_j/a_j}$ are the matrix elements of the dipole moment for the SDT in the q polarization state ($r_q^2 = \sum_k a_{q,k}$), and $p_{q,j} = a_{q,j}/r_q^2$ is the instantaneous probability of state j in the q polarization state.

The next step is to account for the fluctuations of the ionic electric field. The FFM is based on the assumption that an atomic system perturbed by a fluctuating microfield behaves like a set of SDTs that are subject to a stationary Markov mixing process induced by the field fluctuation. This results in an effective exchange between two-level transitions following a Poisson process with a fluctuation rate of $\nu = v_{th}/r_i$ where v_{th} is the ion thermal velocity and r_i is the mean distance between ions. According to Ref. [14], Γ is defined as the diagonal matrix of inverse state lifetimes with $\Gamma_{kj} = \nu\delta_{kj}$ and W as the matrix transition rates between different states, such as $W_{kj} = \nu p_{q,k}$. The expression of the Stark-Zeeman line shape accounting for ion dynamics and polarization is written as

$$I_q(\omega) = \mathrm{Re}\frac{1}{\pi}\sum_{kj} i\langle D_{q,k}|(\omega\mathbf{1} - L^d - i\Gamma + iW)^{-1}|D_{q,j}\rangle p_{q,j}, \qquad (15)$$

which leads to the line shape function for a given transition,

$$I_q(\omega) = \frac{r_q^2}{\pi}\mathrm{Re}\frac{\sum_k \frac{(a_{q,k}+ic_{q,k})/r_q^2}{i(\omega-\omega_{q,k})+\gamma_{q,k}+\nu}}{1-\nu\sum_k \frac{a_{q,k}/r_q^2}{i(\omega-\omega_{q,k})+\gamma_{q,k}+\nu}}. \qquad (16)$$

Thus, the observed Stark-Zeeman profile is the sum given by Eqs. (6)–(8).

If c_k is negligible and if the homogeneous broadening $\gamma_{q,k}$ does not depend on k, Eq. (16) can be written as a functional of the normalized static profile $W_q(\omega)$. The line shape is then expressed as the convolution of a Lorentzian function that represents the homogeneous broadening and the ion dynamic profile,

$$I_q(\omega) = \int d\omega'' \frac{\gamma_q/\pi}{\gamma_q^2 + (\omega-\omega'')^2}\mathrm{Re}\left[\frac{r_q^2}{\pi}\frac{\int \frac{W_q(\omega')d\omega'}{\nu+i(\omega''-\omega')}}{1-\nu\int \frac{W_q(\omega')d\omega'}{\nu+i(\omega''-\omega')}}\right]. \qquad (17)$$

III. RESULTS AND DISCUSSION

In this section, we present calculations of spectral line shapes of hydrogen for conditions relevant to magnetic fusion and argon lines emitted in dense magnetized plasmas.

For the present spectral line shape study, the high-density ($N_e \geqslant 10^{14}$ cm^{-3}) low-temperature ($kT_e \leqslant 10$ eV) tokamak edge plasmas are of particular interest: The optically thin Balmer lines of hydrogen and its isotopes present line profile features that depend directly on plasma properties. For example, odd principal quantum number transitions, such as the H_α line, are useful for determining the magnetic field strength from the measure of the Zeeman components separation. Even principal quantum number transitions, such as the H_β line are useful for determining the electron density from the wings of the Stark line shape [25].

In Fig. 1, we show the Balmer-α (H_α) Stark-Zeeman profiles without Doppler broadening for the plasma conditions $N_e = 10^{15}$ cm^{-3}, $kT_e = kT_i = 10$ eV, and $B = 4$ T. The profiles plotted above and under the abscissa correspond to an observation perpendicular and parallel to the magnetic field, respectively. Two different results are shown: the static profiles (dashed line) and the dynamic profiles (full line). The three Zeeman components (σ_+, π, and σ_-) are clearly distinguishable for an observation perpendicular to **B**, whereas, only the σ components appear for an observation parallel to **B**. The corresponding static line shape presents a plateau in the center of the line, which is explained by the asymmetry of each σ component: As the electric microfield has an arbitrary direction, all M sublevels that fulfill the condition $\Delta M = 0, \pm 1$ are coupled. Emission then appears on the three directions of polarization. In order to understand the ion dynamics effects on the Zeeman components, recall that the general behavior of a set of SDTs undergoing a Markovian mixing process is a collapse of the elements around the gravity center of the set when the fluctuation rate increases. Along this evolution, lines originally inhomogeneous become homogeneous, and their shape can get broader or thinner depending on ν and on the initial SDT distribution. At large ν, the perturbation becomes inefficient, and the line evolves toward the unperturbed shape, here, the pure electron

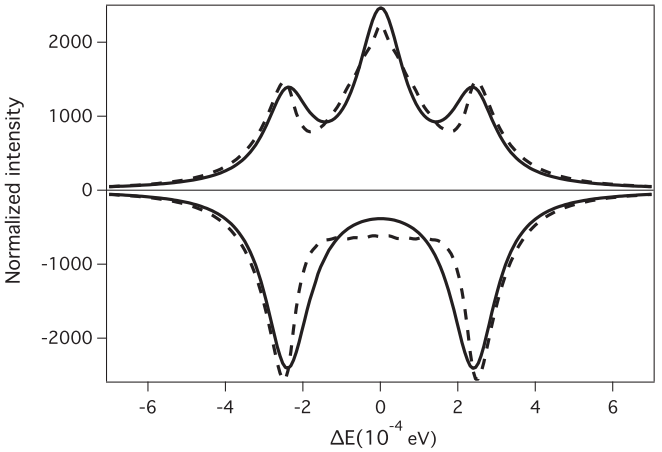

FIG. 1. H_α line shape with an external magnetic field ($B = 4$ T) for $N_e = 10^{15}$ cm^{-3} and $kT_e = kT_i = 10$ eV. Comparison between static profile (dashed line) and dynamic profile (full line). Observation perpendicular to **B** plotted above the abscissa. Observation parallel to **B** plotted under the abscissa.

broadened Zeeman profile. This quite unpredictable response is illustrated in Fig. 1: The π component is symmetric and gets narrower while the σ components, mainly nonsymmetric due to the presence of forbidden components, get shifted and broader for the fluctuation rate relevant to this case.

Figure 2 shows a comparison of the pure electron broadened Zeeman profile (gray curve) of the H_α line, presenting the three σ_+, π, and σ_- components, with dynamic profiles for different values of the fluctuation rate. In order to make a narrowing effect more pronounced, the values of ν were increased up to the value of $100 \times \nu$. The intensity of the line center is set to 1 in order to clearly show the convergence of the dynamic profiles to the pure Zeeman profile as ν increases.

The method presented here is validated by numerical simulation [2] involving hydrogenlike emitters in magnetized plasmas. Numerical simulations play a role as ideal experiments [26], considered as benchmarks. The simulation technique used here relies on (1) the generation of $F_l(t)$ by considering a set of ions and electrons moving along straight trajectories inside a spherical volume (a model of quasiparticles is used [27]) and (2) a fast numerical resolution of Eq. (4) [2,28]. Figure 3 shows the profiles of the H_α line obtained from simulation (circles) and from FFM (full line) for two different values of magnetic field ($B = 2$ T and $B = 4$ T) and for $N_e = 10^{15}$ cm^{-3} and $kT_e = kT_i = 8.5$ eV. Very good

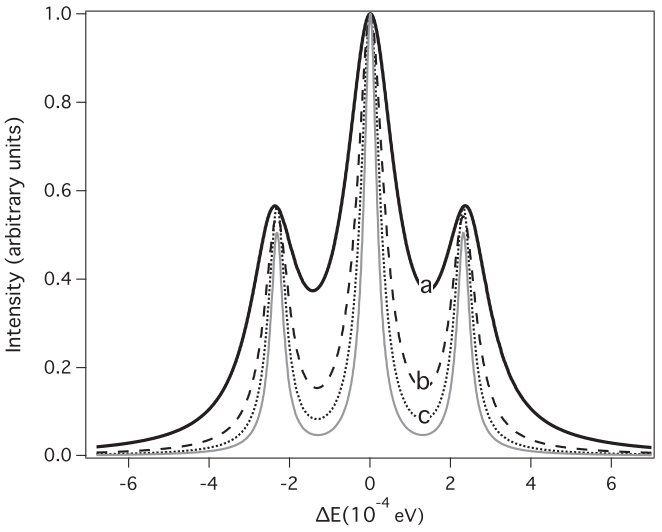

FIG. 2. Comparison of the pure electron broadened Zeeman profile (gray curve) of the H_α line calculated in same conditions as in Fig. 1 with dynamic profiles for different values of the fluctuation rate: ν, 10ν, and 100ν (a)–(c). The observation is perpendicular to **B**.

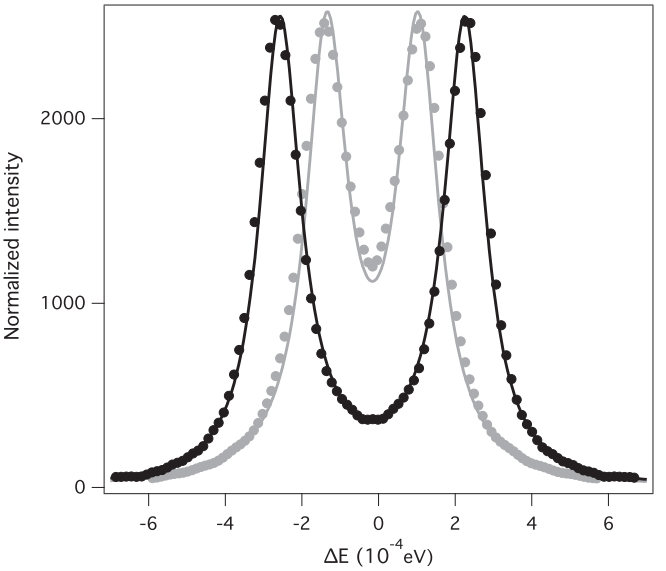

FIG. 3. H_α line shapes with external magnetic fields, $B = 2$ T (gray) and $B = 4$ T (black), for $N_e = 10^{15}$ cm^{-3} and $kT_e = kT_i = 8.5$ eV: FFM (full lines) and numerical simulations (circles). Observation parallel to **B**.

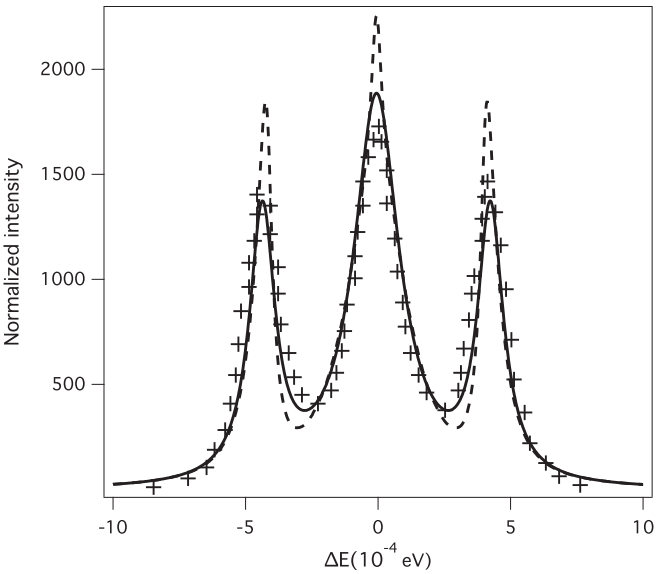

FIG. 4. Comparison between Alcator C-mod multifaceted asymmetric radiation from the edge (MARFE) D_α experimental line (crosses) with the Stark-Zeeman dynamic profile (full line) and the static profile (dashed line) for $N_e = 10^{15}$ cm^{-3}, $kT_e = kT_i = 1$ eV, and $B = 7$ T.

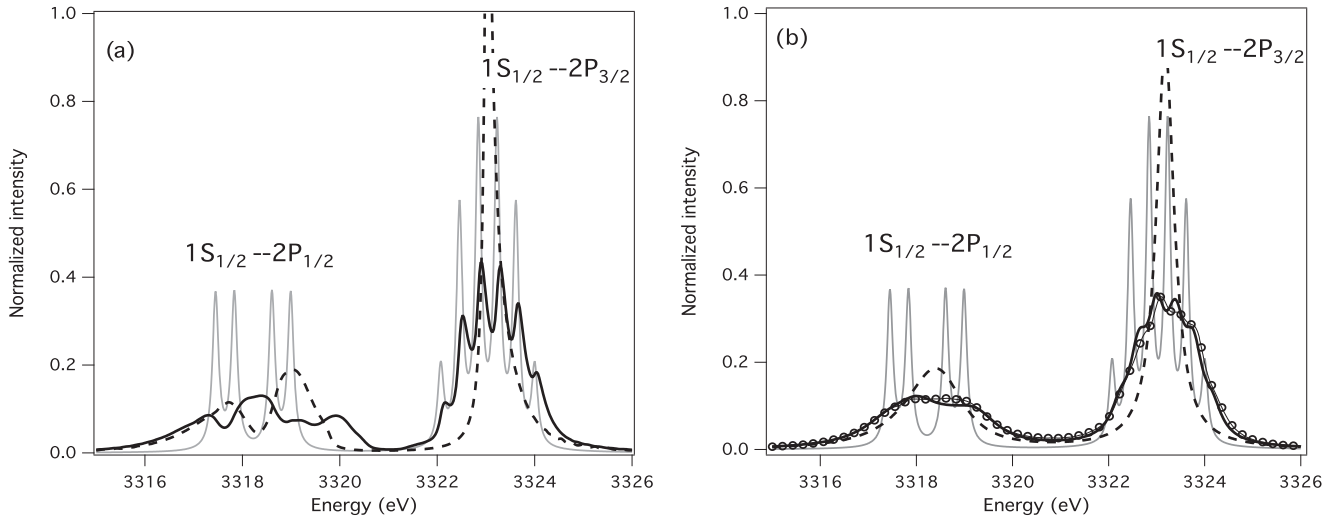

FIG. 5. Ar XVIII Lyman-α line profiles calculated within (a) the quasistatic approximation and (b) accounting for ion dynamics for an external magnetic field $B = 100$ MG and for $N_e = 1.5 \times 10^{23}$ cm^{-3} and $T_e = T_i = 10^7$ K: (gray line) electron broadened Zeeman profile with fine structure, (dashed line) Stark broadened profile, (full line) Stark-Zeeman profile, and (circles) numerical simulations. The direction of observation is perpendicular to **B**.

agreement is found between the simulation and the model. Note that none of these calculations are Doppler broadened and, of course, for such high ionic temperature, the Doppler effect brings an additional broadening.

In the present density range, the Stark-Zeeman profiles are intricate functions of N_e, T_e, and B. To use spectral line profiles as a diagnostic tool, one has to compare the whole measured profile to the whole theoretical one. As, for example, Fig. 4 shows a comparison between the FFM calculated static (dashed line) and dynamic (full line) Stark-Zeeman-Doppler profiles and the D_α (deuterium) line profile (crosses) observed in Alcator C-mod MARFE experiments [25]. The plasma parameters (N_e and T_e) were diagnosed independently and, as in the original paper, the theoretical profiles have not been instrumentally broadened. The dynamic profiles are rather sensitive to electron density variations, and the dynamic profile shows very good agreement with the experimental one for the diagnosed plasma conditions.

The second application concerns Stark-Zeeman line shapes of the Ar XVIII Lyman-α line, accounting for a fine structure calculated for plasma conditions relevant to plasmas produced by laser impact or implosion. In such plasmas, high magnetic fields on the order of 10 to 100 MG have been predicted or have been observed directly [29]. Various physical processes, such as perturbations due to ion microfield, self-generated magnetic field, motional electric field, and Doppler effect, can contribute to the broadening of such highly ionized emitter lines. We have considered a typical laser-driven implosion of a deuterium gas filled microsphere with impurities of argon with a temperature of $T_e = 10^7$ K, an electron density of $N_e = 1.5 \times 10^{23}$ cm^{-3}, and a magnetic field strength of $B = 100$ MG [30]. Even for such high values of magnetic field, the spin-orbit interaction dominates over the effect of the external magnetic field. This case is very advantageous because: First, the profile involves two patterns resulting from both linear and quadratic Stark splitting, respectively, associated with the two fine structure components $1S_{1/2}$-$2P_{1/2}$ and $1S_{1/2}$-$2P_{3/2}$ [14]; second, it presents a strong ion dynamics effect on the Zeeman components. Figures 5(a) and 5(b) show comparisons of the Lyman-α profiles for hydrogenlike argon obtained with pure Zeeman calculations (gray line), pure Stark calculations (dashed line), and Stark-Zeeman calculations (full line) within the quasistatic approximation for the ionic electric field and accounting for the ion dynamics, respectively. Considering the quasistatic case, the four Zeeman components of the $1S_{1/2}$-$2P_{1/2}$ disappear due to the linear Stark effect, whereas, the six Zeeman components of the $1S_{1/2}$-$2P_{3/2}$ are still distinguishable. The characteristic wing at high energies due to the quadratic Stark effect is visible. The ion dynamics effect results in an overall broadening of the line shape. Numerical simulations have been performed using the technique previously described but with electric fields generated by the molecular dynamics technique to account for ion correlations. Here again, comparisons with numerical simulations (circles) give very good agreement.

IV. CONCLUSION

In this paper, we have described a method to account for charged particle dynamics effects in calculations of Stark-Zeeman spectral line shapes. The method, not restricted to simple lines, relies on a reformulation of the FFM, which provides an expression of the dynamic line profile as a functional of the static distribution function of frequencies. Comparisons with numerical simulations and experiments, when they exist, validate the method.

In a first step, the Stark-Zeeman broadened profile is calculated in the quasistatic approximation. Next, the line profile accounting for ion dynamics is calculated via an expression, which depends only on two quantities: the static distribution function and a unique parameter, the fluctuation rate. Here, the method is not limited to a specific atomic physics as the Stark and Zeeman effects are added as perturbations. This highly efficient formalism provides Stark-Zeeman line

shapes for a wide range of density, temperature, and magnetic field values, which is of importance in plasma physics and astrophysics. In addition, this method is numerically fast enough to be implemented in codes that require spectral line shape calculations including all main effects as, for example, in the investigation of radiation effects on plasma transport in plasmas. As shown, spectral line profiles can easily be generated to be used as a diagnostic tool to infer electron density or magnetic field in magnetic fusion devices. Another domain of application is the study of x-ray lines emitted by plasmas produced by laser impact and inertial confinement where high magnetic fields (over 100 MG) can significantly modify the line profile of highly charged ions.

ACKNOWLEDGMENTS

Authors thank the anonymous referees for their very helpful comments and suggestions.

[1] N. Hoe, H. W. Drawin, and L. Herman, J. Quantum Spectrosc. Radiat. Transfer **7**, 429 (1967).
[2] M. Gigosos and M. González, J. Quantum Spectrosc. Radiat. Transfer **105**, 533 (2007).
[3] E. Stambulchik, K. Tsigutkin, and Y. Maron, Phys. Rev. Lett. **98**, 225001 (2007).
[4] J. Rosato, Y. Marandet, H. Capes, S. Ferri, C. Mossé, L. Godbert-Mouret, M. Koubiti, and R. Stamm, Phys. Rev. E **79**, 046408 (2009).
[5] A. Derevianko and E. Oks, Phys. Rev. Lett. **73**, 2059 (1994).
[6] S. Brillant, G. Mathys, and C. Stehlé, Astron. Astrophys. **339**, 286 (1998).
[7] H. R. Griem, *Principles of Plasma Spectroscopy* (Cambridge University Press, Cambridge, UK, 1997).
[8] S. Günter and A. Könies, J. Quantum Spectrosc. Radiat. Transfer **62**, 425 (1999).
[9] L. Godbert-Mouret, M. Koubiti, R. Stamm, K. Touati, B. Felts, H. Capes, Y. Corre, R. Guirlet, and C. De Michelis, J. Quantum Spectrosc. Radiat. Transfer **71**, 365 (2001).
[10] M. L. Adams, R. W. Lee, H. A. Scott, H. K. Chung, and L. Klein, Phys. Rev. E **66**, 066413 (2002).
[11] X. D. Li, S. S. Han, C. Wang, and Z. Z. Xu, J. Quantum Spectrosc. Radiat. Transfer **76**, 31 (2003).
[12] G. Mathys, Astron. Astrophys. **141**, 248 (1984).
[13] L. Godbert-Mouret, J. Rosato, H. Capes, Y. Marandet, S. Ferri, M. Koubiti, R. Stamm, M. González, and M. Gigosos, High Energy Density Phys. **5**, 162 (2009).
[14] A. Calisti, C. Mossé, S. Ferri, B. Talin, F. Rosmej, L. A. Bureyeva, and V. Lisitsa, Phys. Rev. E **81**, 016406 (2010).
[15] A. Calisti, F. Khelfaoui, R. Stamm, B. Talin, and R. W. Lee, Phys. Rev. A **42**, 5433 (1990).
[16] C. A. Iglesias, H. E. DeWitt, J. L. Lebowitz, D. Mac Gowan, and W. B. Hubbard, Phys. Rev. A **31**, 1698 (1985).
[17] R. D. Cowan, *The Theory of Atomic Structure and Spectra* (University of California Press, Berkeley, CA, 1981).
[18] I. P. Grant, B. J. McKenzie, P. H. Norrington, D. F. Mayers, and N. C. Pyper, Comput. Phys. Commun. **21**, 207 (1980).
[19] A. Bar-Shalom, M. Klapisch, and J. Oreg, Phys. Rev. A **38**, 1773 (1988).
[20] M. F. Gu, Can. J. Phys. **86**, 675 (2008).
[21] M. Abramowitz and I. A. Stegun, *Handbook of Mathematical Functions* (Dover, Mineola, NY, 1972).
[22] P. Sauvan and E. Dalimier, Phys. Rev. E **79**, 036405 (2009).
[23] A. Calisti, L. Godbert, R. Stamm, and B. Talin, J. Quantum Spectrosc. Radiat. Transfer **51**, 59 (1994).
[24] C. Mossé, A. Calisti, R. Stamm, B. Talin, R. W. Lee, and L. Klein, Phys. Rev. A **60**, 1005 (1999).
[25] M. L. Adams, H. A. Scott, R. W. Lee, J. L. Terry, E. S. Marmar, B. Lipschultz, A. Y. Pigarov, and J. P. Freidberg, J. Quantum Spectrosc. Radiat. Transfer **71**, 117 (2001).
[26] E. Stambulchik and Y. Maron, High Energy Density Phys. **6**, 9 (2009).
[27] J. Seidel and R. Stamm, J. Quantum Spectrosc. Radiat. Transfer **27**, 499 (1982).
[28] M. Gigosos, M. González, and V. Cardeñoso, Spectrochim. Acta, Part A **58**, 1489 (2003).
[29] J. A. Stamper, Laser Part. Beams **9**, 841 (1991).
[30] M. S. Murillo, M. E. Cox, and S. M. Carr, J. Quantum Spectrosc. Radiat. Transfer **58**, 811 (1997).